Propagating and evanescent properties of double-point defects in sonic crystals

2010 New J. Phys. 12 083024

(http://iopscience.iop.org/1367-2630/12/8/083024)

New Journal of Physics
The open-access journal for physics

Propagating and evanescent properties of double-point defects in sonic crystals

V Romero-García[1,2,4], J V Sánchez-Pérez[1] and L M Garcia-Raffi[3]

[1] Centro de tecnologías físicas: Acústica, Materiales y Astrofísica, Universidad Politécnica de Valencia, Camino de Vera s/n, 46022 Valencia, Spain
[2] Instituto de Ciencia de Materiales, Consejo Superior de Investigaciones Científicas, Sor Juana lnés de la Cruz, 3, Cantoblanco, 28049, Madrid, Spain
[3] Instituto Universitario de Matemática Pura y Aplicada, Universidad Politécnica de Valencia, Camino de Vera s/n, 46022 Valencia, Spain
E-mail: virogar1@mat.upv.es

New Journal of Physics **12** (2010) 083024 (14pp)
Received 22 April 2010
Published 10 August 2010
Online at http://www.njp.org/
doi:10.1088/1367-2630/12/8/083024

Abstract. Complex band structures and multiple scattering theory have been used in this paper to analyze the overlapping of the evanescent waves localized in point defects in sonic crystals (SCs). The extended plane wave expansion (EPWE) with supercell approximation gives the imaginary part of the Bloch vectors that produces the decay of the localized modes inside the periodic system. Double cavities can present a coupling between the evanescent modes localized in the defect, showing a symmetric or antisymmetric mode. When point defects are close, the complex band structures reveal a splitting of the frequencies of the localized modes. Both the real part and the imaginary values of k of the localized modes in the cavities present different values for each localized mode, which gives different properties for each mode. The novel measurements, in very good agreement with analytical data, show experimental evidence of the symmetric and antisymmetric localized modes for a double-point defect in SCs. The investigation of the localization phenomena and the coupling between defects in periodic systems has fundamental importance in both pure and applied physics.

[4] Author to whom any correspondence should be addressed.

Contents

1. Introduction

Periodic distributions of elastic scatterers in an elastic host medium with different physical properties are known as phononic crystals (PCs) [1, 2], and they are the elastic analogues of the well-known photonic crystals [3, 4]. If one of the materials in PCs is a fluid, then the system is called a sonic crystal (SC) [5]. All of these systems present interesting physical properties and recently they have received increasing attention, mainly due to the great number of applications in several branches of physics and engineering [6]–[8]. One of the most important properties of these inhomogeneous materials is the so-called band gaps (BGs): frequency ranges where waves do not propagate through the periodic system. The existence of these BGs leads to several applications; for instance, in the case of SCs, as acoustic filters [9, 10], acoustic barriers [11] or waveguides [12].

In periodic systems, Bloch's theorem and Fourier expansion of the periodic physical properties transform the acoustic wave equation in an eigenvalue problem. The eigenfrequencies $\omega(k)$ for each Bloch's vector k inside the irreducible part of the first Brillouin zone constitute the band structure. This methodology is usually called plane wave expansion (PWE) [13] and it can be used to obtain the so-called band structures, i.e. the propagating modes through the periodic system. The band structures reveal that BGs are ranges of frequencies where no real k exists. It has been shown that the eigenvalues of the problem have real value for the case of SCs [14].

One of the most important properties of the periodic structures is the emergence of localized modes within the BG when a point defect is introduced [9, 15]. A widely used technique in the literature to obtain the effect of creation of point defects in crystals is the supercell approximation in PWE [10, 16, 17]. This approximation gives information only about the propagation nature of the localized modes in the point defects. In these cases, when periodicity is broken or when SCs have finite size, evanescent modes inside the periodic system may appear. Localized modes or modes inside the BG are characterized by evanescent behavior [7, 18, 19]. Then, a more accurate analysis is needed to characterize all the properties of the modes inside the periodic system.

A wave impinging on a complete periodic system with a given frequency ω inside the BG is characterized by complex valued wave numbers $k(\omega)$, which represent the multi-exponential decay of the evanescent mode inside the periodic system [18]. Recent works [20]–[22] show an extension of the PWE (extended plane wave expansion (EPWE)) obtaining the complex part of

the Bloch's waves, revealing that the decay of the modes inside the BG grows as the frequency reaches the center of the BG. In this sense, a localization factor has been defined recently to show this behavior [23]. The localization factor can also be related to recent results that show that, although the decay of these localized modes is multi-exponential, it can be approximated by an exponential-like decay considering only the first harmonic of the Bloch waves in SCs made of rigid cylinders [19].

On the other hand, Sainidou *et al* [24] have introduced a novel extension of the multiple scattering theory (MST) [25] for analyzing slabs that consist of slices of different materials as long as the periodicity parallel to the surface of the slab is preserved. The method, called layer multiple scattering (LMS), allows the study of the scattering problem of slabs that are finite in the direction parallel to the surface of the slab, but infinite in the normal directions to this surface. Alternatively, one can use this method to calculate the complex phononic band structures of an infinite crystal, associated with a given crystallographic plane. In this case, the method provides the propagating and evanescent Bloch waves of the elastic field in the given crystal, corresponding to a given k and a given frequency. LMS has been used to analyze the guidance and quasi-guidance of elastic waves in a glass plate coated on one side with a periodic monolayer of polymer spheres, immersed in water, observing the dispersion diagrams of the interacting modes of the composite slab [26].

The goal of the paper is to analyze the three main characteristics of defect modes in SCs: splitting, symmetry vibrational patterns and evanescent decay of the modes. In addition to PWE, to carry out this study we have used EPWE with supercell approximation, because it is fundamental for the complete understanding of the localized modes. We present the explicit matrix formulation of the supercell approximation in EPWE for N_p point defects. From the complex and real band structures, we observe the splitting and the evanescent behavior of the localized modes inside the BG around the defect. We analyze the localized modes inside multi-point defects, especially in the double-point defect case.

MST in finite SCs is used to analyze the vibrational patterns of the localized modes in a double-point defect. In this case, when the distance between both defects is low enough, it appears as symmetric and antisymmetric vibrational modes similar to the case of a system formed by two masses and three springs, or to the Zeeman effect in the atomic spectra [15]. The novel experimental data that are in good agreement with theory show for the first time the symmetry of the vibrational patterns of localized modes in such a double-point defect. Moreover, we observe the decay of the localized modes outside the double-point defect, in good agreement with the results obtained by EPWE with supercell approximation.

The paper is organized as follows. First of all, we show the main ingredients of the EPWE as well as the explicit matrix formulation of the problem and the extension for a supercell with N_p point defects. After that, the numerical, analytical and experimental results of a double-point defect are shown, giving a complete explanation of the splitting, the symmetry of vibrational patterns and the decay of localized modes. Finally, we give a summary as well as the main conclusions of the work.

2. Extended plane wave expansion (EPWE) with supercell approximation

The analysis of propagating modes can be done by the $\omega(\vec{k})$ formulation, where the existence of BGs is indicated by the absence of bands in determined ranges of frequencies. The mechanism of creation of BGs in finite crystals could be understood by the evanescent behavior of the

modes inside it. At a given frequency ω inside the BGs, the evanescent wave is characterized by a complex valued Bloch vector $\vec{k}(\omega)$ that characterizes the decay of the mode inside the periodic structure. Based on the work of Hsue *et al* [20], recent work by Laude *et al* [21] shows the calculation of complex band structure for PCs. Recently, this work has been extended to the case of SCs for calculations using the supercell approximation [22], which is especially indicated for SCs with point defects. In this section, we present the explicit matrix formulation of the EPWE with supercell approximation to calculate the properties of SCs with N_p point defects inside a supercell. We must take into account that PWE needs low interaction between supercells.

$\omega(k)$ methods are characterized by the next eigenvalue problem,

$$\sum_{\vec{G}'}((\vec{k}+\vec{G})\sigma_k(\vec{G}-\vec{G}')(\vec{k}+\vec{G}')-\omega^2\eta(\vec{G}-\vec{G}'))p_{\vec{k}}(\vec{G}')=0, \tag{1}$$

where $\vec{G}$ is the two-dimensional (2D) reciprocal-lattice vector, k is the Bloch vector and p_k is the pressure. Equation (1) constitutes a set of linear, homogeneous equations for the eigenvectors $p_{\vec{k}(\vec{G})}$ and the eigenfrequencies $\omega(\vec{k})$. We obtain the band structures letting $\vec{k}$ scan the irreducible part of the first Brillouin zone.

Equation (1) can be expressed by the next matrix formulation [13],

$$\sum_{i=1}^{3}\Gamma_i\Sigma\Gamma_i P=\omega^2\Omega P, \tag{2}$$

where $i=1, 2, 3$ and

$$\Sigma=\begin{pmatrix}\sigma(\vec{G}_1-\vec{G}_1) & \dots & \sigma(\vec{G}_1-\vec{G}_{N\times N})\\ \vdots & \ddots & \vdots\\ \sigma(\vec{G}_{N\times N}-\vec{G}_1) & \dots & \sigma(\vec{G}_{N\times N}-\vec{G}_{N\times N})\end{pmatrix}, \tag{3}$$

$$\Omega=\begin{pmatrix}\eta(\vec{G}_1-\vec{G}_1) & \dots & \eta(\vec{G}_1-\vec{G}_{N\times N})\\ \vdots & \ddots & \vdots\\ \eta(\vec{G}_{N\times N}-\vec{G}_1) & \dots & \eta(\vec{G}_{N\times N}-\vec{G}_{N\times N})\end{pmatrix}, \tag{4}$$

$$P=\begin{pmatrix}P(\vec{G}_1)\\ \vdots\\ P(\vec{G}_{N\times N})\end{pmatrix}, \tag{5}$$

where $\vec{G}=(G_1, G_2, G_3)=(2\pi m/a_1, 2\pi n/a_2, 0)$ for the case of the 2D square arrays. If we chose $m=n=(-M, \dots, M)$, the size of the previous matrices is $N\times N=(2M+1)\times(2M+1)$.

From equation (2), we define the next vector,

$$\Phi_i=\Sigma\Gamma_i P. \tag{6}$$

With this definition we can reformulate the eigenvalue problem (2) as the equations system,

$$\begin{aligned}\Phi_i&=\Sigma\Gamma_i P,\\ \omega^2\Omega P&=\sum_{i=1}^{3}\Gamma_i\Phi_i.\end{aligned} \tag{7}$$

In order to obtain an eigenvalue problem for $\vec{k}(\omega)$, we write $\vec{k} = k\vec{\alpha}$, where $\vec{\alpha}$ is a unit vector. Then the Γ_i matrix can be written as

$$\Gamma_i = \Gamma_i^0 + k\alpha_i I, \tag{8}$$

where I is the identity matrix and

$$\Gamma_i^0 = \begin{pmatrix} G_i & 0 & \dots & 0 \\ 0 & G_i & \dots & 0 \\ \vdots & \vdots & \ddots & \vdots \\ 0 & \dots & \dots & G_i \end{pmatrix}, \tag{9}$$

$$\alpha_i = \begin{pmatrix} \alpha_i & 0 & \dots & 0 \\ 0 & \alpha_i & \dots & 0 \\ \vdots & \vdots & \ddots & \vdots \\ 0 & \dots & \dots & \alpha_i \end{pmatrix}. \tag{10}$$

Then, equation (2) can be written in the form of (11), where $\Phi' = \sum_{i=1}^{3} \alpha_i \Phi_i$.

$$\begin{pmatrix} \omega^2\Omega - \sum_{i=1}^{3} \Gamma_i^0 \Sigma \Gamma_i^0 & 0 \\ -\sum_{i=1}^{3} \Sigma \Gamma_i^0 & I \end{pmatrix} \begin{pmatrix} P \\ \Phi' \end{pmatrix} = k \begin{pmatrix} \sum_{i=1}^{3} \Gamma_i^0 \Sigma \alpha_i & I \\ \sum_{i=1}^{3} \Sigma \alpha_i & 0 \end{pmatrix} \begin{pmatrix} P \\ \Phi' \end{pmatrix}. \tag{11}$$

Equation (11) represents a generalized eigenvalue problem with $2N$ eigenvalues k, with possibly complex values. Complex band structures on the incidence direction $\vec{\alpha}$ have been obtained by solving the eigenvalue equation for a discrete number of frequencies and then sorted by continuity of k. In contrast to the $\omega(\vec{k})$ method, in this formulation the periodicity is not relevant and $k(\omega)$ does not follow the first Brillouin zone.

We consider an SC with primitive lattice vectors $\vec{a}_i$ $(i = 1, 2, 3)$. The supercell is a cluster of $n_1 a \times n_2 a \times n_3 a$ scatterers periodically placed in the space. Then, the primitive lattice vectors in the supercell approximation are $\vec{a'}_i = n_i \vec{a}_i$, and the complete set of lattices in the supercell approximation is $\{R' | R' = l_i \vec{a'}_i\}$, where n_i and l_i are integers. The primitive reciprocal vectors are then

$$\vec{b'}_i = 2\pi \frac{\varepsilon_{ijk} \vec{a'}_j \times \vec{a'}_k}{\vec{a'}_1 \cdot (\vec{a'}_2 \times \vec{a'}_3)}, \tag{12}$$

where ε_{ijk} is the 3D Levi–Civita completely anti-symmetric symbol. The complete set of reciprocal lattice vectors in the supercell is $\{\vec{G} | \vec{G}_i = N_i \vec{b'}_i\}$, where N_i are integers.

The density ρ_i and the bulk modulus B_i are the physical properties involved in the wave equation and, using the Fourier expansion and the geometry of the system, they can be expressed in terms of the structure factor for the PWE (EPWE) as well as for the PWE (EPWE) with supercell approximation. The index $i = (h, c)$ represents the host medium and the scatter, respectively. The filling fraction of a cylinder in a supercell is $f = \pi r^2 / A$, where A is the area occupied by the supercell. If we consider that β_i represents the values (ρ_i^{-1}, B_i^{-1}) and that the

supercell has N_c cylinders organized in an array of size $n_1 a \times n_2 a$, then

$$\beta(\vec{G}) = \begin{cases} \beta_c N_c f + \beta_h (1 - N_c f) & \text{if } \vec{G} = \vec{0}, \\ (\beta_c - \beta_h) F(\vec{G}) & \text{if } \vec{G} \neq \vec{0}, \end{cases} \tag{13}$$

where $F(\vec{G})$ is the structure factor of the supercell.

In this approximation, the structure factor of the supercell has to be computed taking into account the size of the supercell. If we consider a 2D SC with cylindrical scatterers with radius r and size of the supercell $n_1 a \times n_2 a$, the structure factor of the supercell is expressed by

$$F(\vec{G}) = \sum_{i=-(n_1-1)/2}^{(n_1-1)/2} \sum_{j=-(n_2-1)/2}^{(n_2-1)/2} e^{\imath(ia|\vec{G}_1| + ja|\vec{G}_2|)} P(\vec{G}), \tag{14}$$

where

$$P(\vec{G}) = \frac{2f}{Gr} J_1(G), \tag{15}$$

and where a is the lattice constant inside the supercell and $G = |\vec{G}|$.

Previous equations show the expressions for the approximation of the complete supercell. If the supercell presents N_p point defects at the sites labeled (l_s, m_s) in the periodic system, with $s = 1, \ldots, N_p$, then the Fourier coefficients of the expansions of the physical parameters involved in the problem follow the next equation,

$$\beta(\vec{G}) = \begin{cases} \beta_c (N_c - N_p) f + \beta_h (1 - (N_c - N_p) f & \text{if } \vec{G} = \vec{0}, \\ (\beta_c - \beta_h) F(\vec{G}) & \text{if } \vec{G} \neq \vec{0}. \end{cases} \tag{16}$$

The structure factor of such a supercell with N_p point defects is

$$F(\vec{G}) = \left(\sum_{i=-(n_1-1)/2}^{(n_1-1)/2} \sum_{j=-(n_2-1)/2}^{(n_2-1)/2} e^{\imath(ia|\vec{G}_1| + ja|\vec{G}_2|)} - \sum_{s=1}^{N_p} e^{\imath(l_s a|\vec{G}_1| + m_s a|\vec{G}_2|)} \right) P(\vec{G}). \tag{17}$$

The interaction of the defect points in the supercell approximation must be as low as possible between the neighboring supercells in order to decrease the overlap between defects. Thus the size of the supercell should be big enough to place the point defects separated in consecutive supercells.

Introducing the previous expressions in the matrices of the PWE (2) or the EPWE (11), we can calculate the real and complex band structures. In the present paper, we analyze the case of a double-point defect in a square array at sites $(1, 0)$ and $(-1, 0)$ in a supercell of $11a \times 11a$. In this situation, the distance between defects is equal to $2a$ and the distance between two double-point defects in different supercells is equal to $20a$.

3. EPWE results: localized modes

Since Sigalas [9] studied the defect mode produced by a point defect in periodic structures, several kinds of defects have been analyzed in the last few years, showing in all cases the localization of sound for frequencies inside the BG [15, 27, 28]. Experimental and numerical analyses of the localization in a point defect considered as a cavity inside the SC have been reported recently by Wu *et al* [29, 30] and Zhao *et al* [17, 31], showing the dependence of

localization on the size of the crystal and on the filling fraction (the bigger the size and the filling fraction, the bigger the localization in the cavity). Moreover, when we consider two-point defects, coupling between localized modes in each defect point is possible [32, 33]. An accurate interferometric setup has been used by Russell *et al* [33] for observing the coupled states in a double-point defect, noting the evidence for odd and even symmetry trapped states in a new class of ultra-efficient photosonic devices in which both sound and light are controlled with great precision and their interactions enhanced. For the case of double-point defects, the bigger the distance between cavities, the lower the coupling between defect points.

In this section, we show novel results regarding the imaginary part of the Bloch vector for the localized modes inside the SC with multi-point defects. The localization of waves inside these defects is mainly characterized by three properties. Firstly, the modes are separated in the frequency domain, i.e. there is a splitting of the localization frequency if the point defects are close enough. Secondly, the modes present symmetries in the vibrational pattern depending on the number of vacancies in the crystal. Thirdly, the localized modes are evanescent and they decay outside the defect but inside the SC. Without loss of generality, we show the results of a double-point defect in very good agreement with the experimental data, showing the symmetric and antisymmetric vibrational patterns of the localized modes. Evidently, the oscillation modes of N-point defects with $N > 2$ will present more complicated vibrational patterns than the ones appearing in the double-point defect; then they cannot be classified into such simple modes as symmetric and antisymmetric ones.

The complex and real band structures reveal that the values of k for the localized modes are characterized by a real value of k and it is related to the localization frequency. However, this localized mode presents evanescent behavior out of the defect, because it is surrounded by a perfect periodicity; thus, the excited mode in the surrounding crystal by the localized mode presents an imaginary k that is related to the evanescent behavior of the mode outside the point defects [19]. The rest of the modes inside the BG only present the imaginary part; then they are killed inside the crystal because of their evanescent behavior.

3.1. Splitting of localized modes

In order to analyze the splitting of the localized modes, we have calculated the real and complex band structures of an SC with a double-point defect using EPWE with supercell approximation using a supercell of size $11a \times 11a$. We consider a 2D SC consisting of PVC cylinders of radius r in air background arranged in a square lattice with lattice constant a. The material parameters employed in the calculations are $\rho_{\text{air}} = 1.23\,\text{kg}\,\text{m}^{-3}$, $\rho_{\text{PVC}} = 1400\,\text{kg}\,\text{m}^{-3}$, $c_{\text{air}} = 340\,\text{m}\,\text{s}^{-1}$ and $c_{\text{PVC}} = 2380\,\text{m}\,\text{s}^{-1}$. We consider a filling fraction $f = \pi r^2/a^2 \simeq 0.65$. For the calculations, we have used $N = (2 \times 15 + 1)^2 = 961$ plane waves. Several calculations have been carried out in order to obtain a good convergence of the solution. This number of plane waves is bigger than the one used in previous works [21] and provides a good convergence of the solution of the eigenvalue problem.

A mode within the BG in an infinite SC without defects is characterized by a pure imaginary value of $k = \text{i}k_{\text{im}}$ (where $k_{\text{im}} = \text{Im}(k)$) [19, 21, 23]. In figure 1(a) (left panel), we can observe the dependence of $\text{Im}(k)$ on k for a complete SC within the BG for the ΓX direction. We can observe a maximum value of $\text{Im}(k)$ for the frequency in the midgap (926 Hz), which means that the imaginary part of the wave number for frequencies inside the BG grows with values of frequency closer to the center of the BG and disappears at the edges of the BG, i.e. the

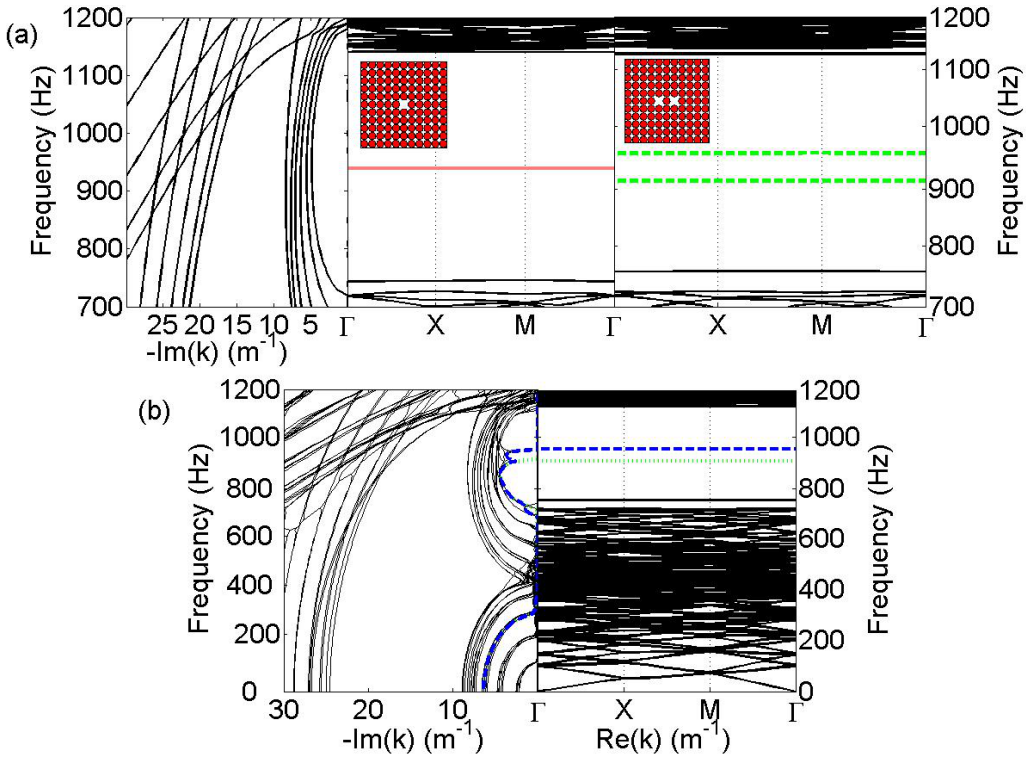

Figure 1. Real and complex band structures for a sonic crystal (SC) with point defects. (a) Left: complex band structure of a complete SC calculated by extended plane wave expansion (EPWE) with supercell approximation. Center: band structures calculated by PWE with supercell approximation of a SC with a point defect; the continuous red line represents the defect mode. Right: band structures for a SC with a double-point defect; the dashed green line represents the defect modes of a double-point defect. Insets show the supercell used in the calculations. (b) Complex and real band structures of a double-point defect.

rate of decay is bigger for frequencies closer to the center of the BG [7, 19, 23]. Modes within the BG decay inside the SC because of their evanescent behavior [19].

In contrast to the modes in the BG, localized modes can travel up to the point defect where the wave is localized. Figure 1(a) (central and right panels) represents the real band structures calculated by PWE with supercell approximation for both a SC with a point defect (central) and a SC with a double-point defect (right). We can observe the localized mode generated by a point defect in a SC at the frequency $\nu_0 = 932$ Hz, whereas the frequencies of the localized modes of a double-point defect have been split (right panel of figure 1(a)). The frequencies of the two localized modes due to the double-point defect split around the localized mode of a single defect: one with a lower frequency, $\nu_1 = 910$ Hz, than the corresponding frequency of the localized mode in a single defect, and another one, $\nu_2 = 958$ Hz, with a higher frequency than the single defect. This phenomenon is analogous to the splitting of the degenerate atomic levels in diatomic molecules.

The splitting in two peaks may be understood qualitatively by considering that the double cavity in the double-point defect is coupled forming a large cavity with two resonant

frequencies. When a wave with one of these frequencies impinges on the crystal from outside, the double-point defect is sawn and the wave penetrates into the cavity. Then, the borders of the cavity act as perfect mirrors, producing the localization of the wave inside the cavity. This results in a coupling inside the double-point defect, producing two localized modes depending on the distance between the point defects [15, 17, 32].

Because the splitting depends on the distance and on the shape of the multi-point defect, one can study the vibrational patterns that appear inside the multi-point defect, analyzing the differences in frequency of the localized modes. The factor $(\nu_1 - \nu_2)/\nu_0$ indicates how the splitting will be produced. For big values of this factor, one can expect modes separated in frequencies (as many as single-point defects constituting the multi-point defect), whereas a small factor represents a weak overlap between the point defects in the multi-point defect, which produces narrow splitting.

The complex band structures give us additional information about the properties of the localized modes. Figure 1(b) represents the complex (left panel) and the real (right panel) band structures for an SC with a double-point defect. For each localized mode, a determined imaginary k becomes a pure real value, in good agreement with the results of the PWE with supercell approximation. This real part is related to the wave vector for the localization frequency, whereas the imaginary part of the localized mode is related to the rate of decay outside the defect but inside the SC. As we have seen, the localized modes in the double-point defect are distributed around the localized mode of a single-point defect. However, the localized mode of the single-point defect appears a little above the midgap frequency (926 Hz). Thus, it is expected that the imaginary part of the localized modes of double-point defects will present different values for each mode and, as a consequence, each mode presents different evanescent behaviors outside the defect (see figure 1(b)). This prediction of the EPWE will be used for distinguishing experimentally the symmetric with respect to the antisymmetric modes.

3.2. Symmetric and antisymmetric modes

The previous discussion about the splitting of the modes in multi-point defects does not provide information about how the modes are localized or what is the distributed field inside the double cavity. This will be discussed now.

The results obtained by PWE or EPWE for the localized modes could be used to plot the modal shapes for the defect modes using the eigenvectors. However, these modal shapes do not take into account the effect of the finite size of the crystal. Thus, to compare with experimental data corresponding to a SC of finite size, in this section, we have calculated the modal shapes inside the double defect using MST. MST provides complementary information with respect to that provided by EPWE in the case of the infinite structures.

MST [34, 35] has been used to analyze the pressure field inside a SC with point defects. A SC of $7a \times 5a$ size with $a = 0.22$ m of rigid cylinders with radius $r = 0.1$ m is considered in this section. We have generated a double-point defect with individual defect points separated by a distance $d = 2a$. We have considered this size because of the experimental restrictions and to be able to compare both theoretical and experimental data.

For the crystal considered in this section, the frequencies of the localization modes differ a bit with respect to the ones calculated by PWE and EPWE with supercell approximation. We have to take into account that, in this case, we consider a finite crystal, and, as it has been shown in the literature, the localization frequencies depend on the size of the crystal as well as the filling

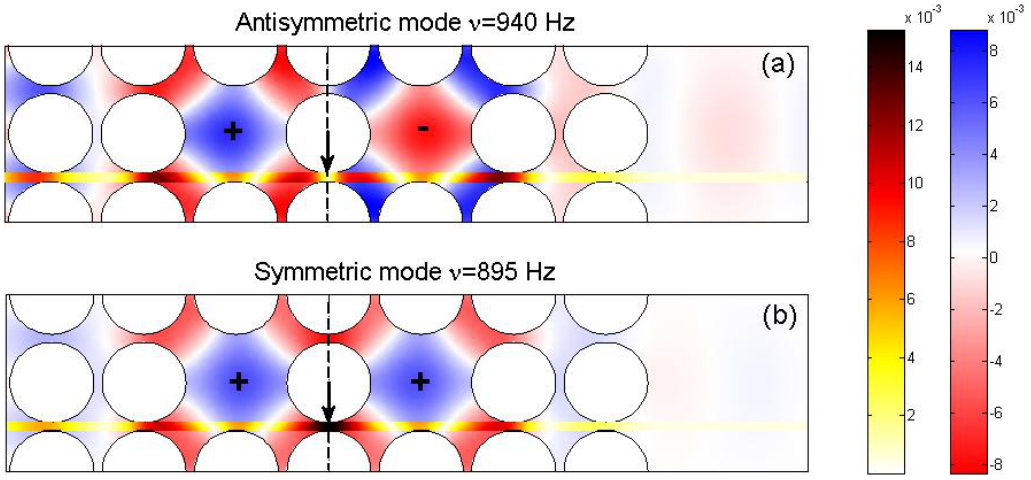

Figure 2. Pressure maps of a double-point defect separated by a distance $d = 2a$. The value $|p|$ between two rows of the SC containing the point defects is also plotted. Pressure map of the antisymmetric (a) and symmetric (b) coupling of the localized modes inside the double-point defect. Arrows represent the values of $|p|$ in the midpoint (dashed line) between two rows of cylinders containing the double-point defect.

fraction, and on the number of rows around the defect. In this case, the localization frequency for the antisymmetric mode is $\nu_1 = 940$ Hz, and that for the symmetric mode is $\nu_2 = 895$ Hz. These frequencies represent the maximum values of the acoustic spectra inside the point defects. Note the small difference with respect to the ones obtained by PWE and EPWE.

The pressure fields calculated by MST inside the SC with a double-point defect for the localization frequencies are shown in figure 2. We can observe that the pressure field for the mode with high frequency has an antisymmetric pattern (figure 2(a)), whereas the pressure field for the mode with low frequency has a symmetric pattern (figure 2(b)).

In figure 2, one can also observe the values of $|p|$ for the space between two rows of the SC containing the double-point defect. The vibrational patterns of the defect modes in a double-point defect are characterized with respect to a symmetry plane (see the dashed line in figure 2) situated just in the midpoint between two defects in the double-point cavity. There is a symmetric mode and an antisymmetric mode with respect to this plane. The symmetric vibrational mode is characterized by a vibration in phase of the pressure field in each point defect, whereas the antisymmetric mode is characterized by a vibration of the pressure field with opposition of phase. Because of these properties, the point just in the symmetry plane presents different values of $|p|$ for each localized mode (see arrows in figure 2). For the antisymmetric mode (figure 2(a)), one can observe a minimum value of $|p|$ at this point, whereas one can find a maximum value for the symmetric mode (figure 2(b)).

Experimental results inside the SC have been performed in an echo-free chamber of dimensions $8 \times 6 \times 3\,\mathrm{m}^3$. In order to obtain the experimental dependence of the pressure all along the SC, we have measured the pressure field in several points between two rows of the SC containing the double-point defect. The experimental SC has been made of 1 m long cylinders of PVC. The size of the SC considered in this work has adequate dimensions to be capable of introducing the microphone between rows. The microphone used is a prepolarized free-field

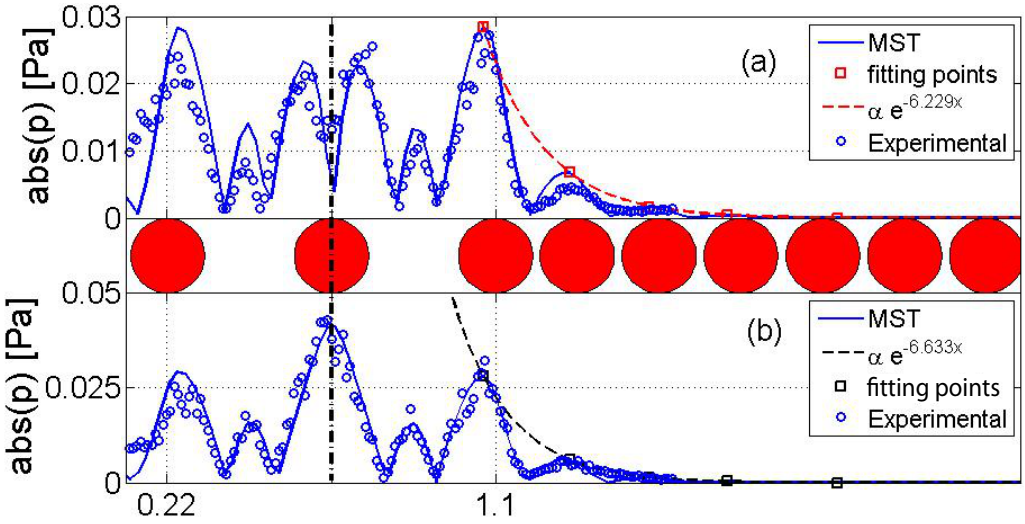

Figure 3. Numerical (continuous line) and experimental (open circles) profiles of the $|p|$ between two rows containing the double-point defect (see figure 2). (a) Antisymmetric mode ($\nu = 940$ Hz) and (b) symmetric mode ($\nu = 895$ Hz). The dashed line represents the exponential decay of the localized modes outside the double-point defect fitted from the maximum values of the analytical data represented by square open points. The border of the double-point defect is marked with a dotted line.

$1/2''$ type 4189 B&K. The diameter of the microphone is 1.32 cm, which is approximately $0.06a$, so the influence over the pressure field measured is negligible.

With our system 3DReAMS (3D Robotized e-Acoustic Measurement System), it is possible to sweep a 3D grid of measuring points located at any trajectory inside the echo-free chamber. Motion of the robot is controlled by NI-PCI 7334 . We have analyzed the absolute value of the sound pressure between two rows of the SC moving the microphone in steps of 1 cm.

Figure 3 shows the values of $|p|$ obtained by MST versus the ones measured experimentally. The experimental results are in very good agreement with the ones obtained with MST. Note the different values of $|p|$ in the midpoint. As MST predicted, a maximum is observed for the symmetric mode at $\nu = 895$ Hz (figure 3(b)) and a minimum for the antisymmetric mode at $\nu = 940$ Hz (figure 3(a)). The good agreement between theoretical (MST) and experimental results is worth noting. These measurements constitute the first experimental evidence of symmetric and antisymmetric vibrational modes inside a SC with a double-point defect.

3.3. Decay of the localized modes

Due to the mode of a single-point defect being a little above the midgap, one can observe in figure 1(b) that the localized modes in a double point defect present different imaginary parts of k: the values of the imaginary part of k for the antisymmetric mode are lower than the ones corresponding to the symmetric mode, i.e. the rate of decay outside the cavity of the symmetric mode must be bigger than that of the antisymmetric case. In figure 3, one can observe the decay

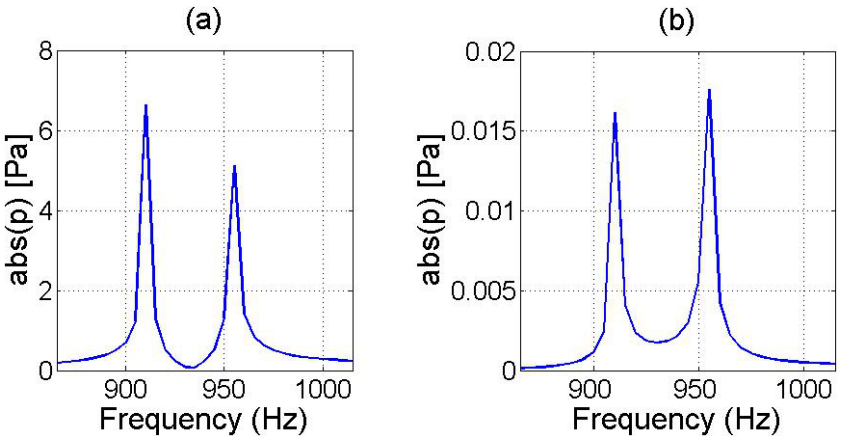

Figure 4. Spectra for a SC made of PVC $9a \times 5a$ cylinders with a lattice constant $a = 0.22$ m in a square array with a double-point defect. (a) Spectrum measured inside one of the point defects in the double-point defect. (b) Spectrum measured outside the crystal at a distance $10a$ from the start of the SC.

of the localized modes outside the double-point cavity. The border of the double-point defect is marked by dotted lines.

In order to analyze the decay of the modes outside the cavity, we have studied the behavior of the maximum analytical values of $|p|$ outside the cavity (see open squares in figure 3), calculated by MST in a SC of rigid cylinders with size $11a \times 5a$. Although the decay of the modes outside the cavity is multi-exponential [18], we can fit these values to an exponential-like $a\,e^{bx}$ for analyzing the differences in the rate of decay due to the differences in the imaginary part of k for each localized mode.

Both the fitted exponential decays are represented in figure 3 (dashed lines). The decay rate for the antisymmetric mode is $b = -6.229 \pm 0.237\,\mathrm{m}^{-1}$, whereas the decay rate for the symmetric mode is $b = -6.633 \pm 0.178\,\mathrm{m}^{-1}$. Thus, as was discussed for the results obtained in the previous section by EPEWE with supercell approximation, because of the symmetric distribution of the frequencies of the localized modes in a double-point defect with respect to the localized mode in a single cavity, the decay rate of the antisymmetric mode in a double-point defect must be lower than that of the symmetric mode. On the other hand, we can observe that the values of the decay rate of the symmetric and antisymmetric modes are similar and the difference between them is small. The splitting of the frequencies of the localized modes in a double-point defect around the frequency of the single cavity implies that the rates of decay in double-point defects have to be different, but also one of them should be smaller than the other because its distance to the center of the gap is bigger.

In finite crystals, where the localized modes can travel outside the periodic structure because of their evanescent behavior, the previous results indicate that the symmetric mode will be killed more easily than the antisymmetric mode. Thus, the design of filters based on SCs with point defects should take into account these kind of results. In figure 4(a), we represent the spectrum inside a point defect in a SC with a double-point defect. In this case, we can observe that the value of pressure of the peak of the symmetric mode (lower frequency) is higher than that for the peak of the antisymmetric mode. In figure 4(b), we represent the spectra for the same SC with a double-point defect but measured outside the SC at a distance $10a$ from the beginning

of the SC. One can observe that the values of pressure for the symmetric mode are lower than the values of the antisymmetric mode. Thus, the symmetric mode has been more damped by the crystal out of the double-point defect than the antisymmetric mode. Similar results can be observed in figure 2, where the acoustic field behind the crystal for the antisymmetric mode is a bit bigger than the corresponding one for the symmetric mode. These results are in complete agreement with the differences in the imaginary part of k. Moreover, the difference in the value of the imaginary of the complex wave vector is direct evidence of the existence of different vibrational modes in multi-point defects and reveals the existence of a coupling between them.

4. Conclusions

Usual calculations with PWE, $\omega(k)$ methods, do not provide any information about the evanescent behavior of the localized modes in point defects inside periodic structures. In this work, we present an explicit matrix formulation of EPWE with supercell approximation for a supercell with N_p point defects for SCs. This technique allows us to study the evanescent behavior of the modes inside a SC with multi-point defects. Localized modes in SCs are mainly characterized by three properties: splitting of frequencies, the symmetry of the vibrational patterns and evanescent behavior inside the crystal. EPWE in addition to PWE both with supercell approximation has been used to analyze the whole properties of the localized modes in a SC with a double-point defect. First we analyze the splitting produced by the generation of a double-point defect, showing the effects in both the real and imaginary band structures. From the imaginary complex band structure, we find that the localized modes present different values for the imaginary part of k, which means that each mode has a different decay rate inside the crystal. This property has been observed experimentally by fitting the exponential decay for each localized mode inside the crystal. The symmetry of the vibrational patterns in a double-point defect has also been analyzed in the paper by means of MST calculation and experimental data. The novel experimental evidence shows the symmetric and antisymmetric vibrational patterns in SCs with double-point defects. These data are in very good agreement with analytical data. Finally, using the different decay rates of both vibrational modes, we confirm our conclusions giving a new methodology to determine different vibrational modes in periodic media. This work shows the basis for the correct understanding of the design of narrow filters and wave guides based on periodic structures with multi-point defects.

Acknowledgments

This work was supported by MEC (the Spanish Government) and FEDER funds through grants MAT2009-09438 and MTM2009-14483-C02-02.

References

[1] Sigalas M and Economou E 1993 *Solid State Commun.* **86** 141
[2] Kushwaha M, Halevi P, Dobrzynski L and Djafari-Rouhani B 1993 *Phys. Rev. Lett.* **71** 2022
[3] Yablonovitch E 1987 *Phys. Rev. Lett.* **58** 2059
[4] John S 1987 *Phys. Rev. Lett.* **58** 2486
[5] Martínez-Sala R, Sancho J, Sánchez-Pérez J V, Gómez V, Llinares J and Meseguer F 1995 *Nature* **378** 241
[6] Khelif A, Wilm M, Laude V, Ballandras S and Djafari-Rouhani B 2004 *Phys. Rev.* E **69** 067601

[7] Joannopoulus J D, Johnson S G, Winn J N and Meade R D 2008 *Photonic Crystals: Molding the Flow of Light* (Princeton, NJ: Princeton University Press)
[8] Sigalas M, Kushwaha M S, Economou E N, Kafesaki M, Psarobas I E and Steurer W 2005 *Z. Kristallogr.* **220** 765–809
[9] Sigalas M 1997 *J. Acoust. Soc. Am.* **101** 1256
[10] Sigalas M 1998 *J. Appl. Phys.* **84** 3026
[11] Sánchez-Pérez J V, Rubio C, Martínez-Sala R, Sánchez-Grandia R and Gómez V 2002 *Appl. Phys. Lett.* **81** 5240
[12] Vasseur J O, Deymier P A, Djafari-Rouhani B, Pennec Y and Hladky-Hennion A C 2008 *Phys. Rev.* B **77** 085415
[13] Kushwaha M, Halevi P, Martnez G, Dobrzynski L and Djafari-Rouhani B 1994 *Phys. Rev.* B **49** 2313–22
[14] Hernández-Cocoletzi H, Krokhin A and Halevi P 1995 *Phys. Rev* B **51** 17181–3
[15] Li X and Liu Z 2005 *Solid State Commun.* **133** 397402
[16] Wu F, Hou Z, Liu Z and Liu Y 2001 *Phys. Lett.* A **292** 198
[17] Zhao Y and Yuan L B 2009 *J. Phys. D: Appl. Phys.* **42** 015403
[18] Engelen R, Mori D, Baba T and Kuipers L 2009 *Phys. Rev. Lett.* **102** 023902
[19] Romero-García V, Sánchez-Pérez J V, Castiñeira Ibáñez S and Garcia-Raffi L M 2010 *Appl. Phys. Lett.* **96** 124102
[20] Hsue Y, Freeman A and Gu B 2005 *Phys. Rev.* B **72** 195118
[21] Laude V, Achaoui Y, Benchabane S and Khelif A 2009 *Phys. Rev.* B **80** 092301
[22] Romero-García V, Sánchez-Pérez J V and Garcia-Raffi L M 2010 arXiv:1001.3758
[23] Wang Y, Li F, Kishimoto K, Wang Y and Huang W 2009 *Eur. Phys. J.* B **67** 501–5
[24] Sainidou R, Stefanou N, Psarobas I and Modinos A 2005 *Comput. Phys. Commun.* **166** 197–240
[25] Psarobas I E, Stefanou N and Modinos A 2000 *Phys. Rev.* B **62** 278
[26] Sainidou R and Stefanou N 2006 *Phys. Rev.* B **73** 184301
[27] Wu F, Zhong H, Zhong S, Liu Z and Liu Y 2003 *Eur. Phys. J.* B **34** 265–8
[28] Zhong H, Wu F, Zhang X and Liu Y 2005 *Phys. Lett.* A **339** 478–87
[29] Wu L, Chen L and Liu C 2009 *Physica* B **404** 1766
[30] Wu L Y, Chen L W and Liu C M 2009 *Phys. Lett.* A **373** 1189–95
[31] Zhao Y C, Wu Y B and Yuan L B 2009 *Phys. Scr.* **80** 065401
[32] Khelif A, Choujaa A, Djafari-Rouhani B, Wilm M, Ballandras S and Laude V 2003 *Phys. Rev.* B **68** 214301
[33] Russell P S J, Marin E, Dez A, Guenneau S and Movchan A B 2003 *Opt. Express* **11** 2555
[34] Linton C and McIver P 2001 *Handbook of Mathematical Techniques for Wave/Structure Interactions* (London: Chapman and Hall)
[35] Chen Y Y and Ye Z 2001 *Phys. Rev.* E **64** 036616